

**DESIGN OF LOW PHASE NOISE VERY HIGH FREQUENCY (VHF) LOW
BAND VOLTAGE CONTROLLED OSCILLATOR (VCO) FOR
TRANSCEIVER APPLICATION**

by

YEAP KIM HUAT

**Thesis submitted in fulfilment of the requirements for the degree of
Masters of Science**

September 2011

DECLARATION

I hereby declare that the work in this thesis is my own except for quotations and summaries which have been duly acknowledged.

5th September 2011

YEAP KIM HUAT

S-LM0403

AKNOWLEDGEMENT

It has been a great honor to be granted the opportunity to undergo my postgraduate research in School of Electronic and Electrical Engineering of Universiti Sains Malaysia.

First and foremost, I would like to dedicate my sincerest acknowledgement towards my supervisor, Associate Professor Dr. Widad Ismail, for her invaluable guidance and advises throughout my research. As a part-time researcher, my session in meeting up with my supervisor has not been much often, but the inputs she provided during every session have been very fruitful. In times of difficulties faced during my research, there is no other but only my supervisor that I could refer to, in which I really feel blessed about. With her vast knowledge and experience in the research communication field, her advices have continuously helped me channeled through the challenges I encountered.

My earnest gratitude to my parents, my twin brother, my sister in law, my wife, and my daughter, weighs no lesser. The sophisticated journey in striving through the research has been rather enduring. I have to admit that I almost cross the boundary of giving up, have it not for the undivided and consistent support from them. I could not but feel grateful and touched, when my negligence to them was returned by their love and motivation, which turn out to be the bank of strength for me to navigate through all hindrances I faced in my research.

No word could express the deep gratitude that blossoms in my heart. THANK YOU VERY MUCH!

TABLE OF CONTENTS

	PAGE
DECLARATION	ii
AKNOWLEDGEMENT	iii
TABLE OF CONTENTS	iv
LIST OF TABLES	xi
LIST OF FIGURES	xiv
LIST OF ABBREVIATIONS	xxviii
ABSTRAK	xxxii
ABSTRACT	xxxiii
CHAPTER 1 INTRODUCTION	1
1.1 Background	1
1.2 Applications of VHF Low Band	2
1.3 Advantages of VHF Low Band	3
1.3.1 Precise Transmission	3
1.3.2 Extensive Coverage	4
1.3.3 Ample Spectrum Availability	4
1.3.4 Exemption from Narrow Band Requirements	4
1.4 Problem Statement	5
1.5 Research Objectives	6
1.6 Requirements	7
1.7 Research Scopes and Limitations	10
1.8 Research Contribution	11

1.9	Thesis Organization	12
CHAPTER 2 LITERATURE SURVEY		13
2.0	Introduction	13
2.1	Noise	13
2.1.1	Thermal Noise	14
2.1.2	Shot Noise	15
2.1.3	Flicker Noise	16
2.2	Phase Noise	17
2.2.1	Leeson's Model	20
2.2.2	Linear Time Invariant (LTI) Model	23
2.2.3	Lee and Hajimiri's Model	28
2.2.4	Samori's Model	33
2.2.5	Demir's Model	41
2.3	Existing VCO Phase Noise Improvement Techniques	44
2.3.1	High Q Resonant Circuit	44
2.3.2	Selection of Oscillator Device	45
2.3.3	Increasing Area of Transistor	45
2.3.4	Sufficient Oscillator Power Output	46
2.3.5	Sufficient Feedback Level	46
2.3.6	Increase Core Current	46
2.3.7	Power Line Rejection	47
2.3.8	Filtering at Steering Line	48
2.3.9	Capacitive Filtering at The Tail Current Source	49
2.3.10	LC Filtering Technique	50

2.3.11	Remove Tail Current Source	51
2.3.12	Reduce VCO Sensitivity K_v by Switched Capacitors	51
2.3.13	Differential Steering Voltage Control	53
2.4	Previous Works	54
2.5	Summary	55
CHAPTER 3 RESEARCH METHODOLOGY		57
3.1	Introduction	57
3.2	Design Methodology	57
3.3	VHF Low Band VCO Block Design	60
3.4	Oscillator Design and Mathematical Model Derivations	61
3.5	ADS Overview	70
3.5.1	Lump Component Model	70
3.5.2	RF Component Model	71
3.5.3	Momentum Component Model	71
3.6	PCB Layout and Momentum Model	72
3.7	Components Selection and Design Configuration for Low Phase Noise	81
3.7.1	Varactor Diode	81
3.7.2	Back-to-Back Varactor Diode	85
3.7.3	Low Noise Bypass Capacitor	86
3.7.4	RF Bypass Capacitor	86
3.7.5	RF Choke	87
3.7.6	Ferrite Bead	89
3.7.7	JFET Transistor	90

3.7.8	Low Noise Biasing Design	92
3.7.9	Linearizing Inductor Design	93
3.7.10	Schottky Diodes AGC Design	97
3.8	Test and Measurement Methodology	97
3.8.1	S-Parameter Measurement Methodology	97
3.8.2	VCO Parametric Test Methodology	98
3.8.2.1	Frequency Response, Guard Band, Sensitivity, Power Level Test	99
3.8.2.2	Phase Noise Test	100
3.8.2.3	Second Harmonics Output and Feedback Power Test	101
3.8.2.4	Hum and Noise Test	102
3.9	Summary	103
CHAPTER 4 DESIGN AND SIMULATION		104
4.1	Introduction	104
4.2	Oscillator Design	104
4.2.1	Rx Oscillator Calculation	107
4.2.2	Rx Oscillator Lump Component Model Simulation	108
4.2.3	Rx Oscillator RF Component Model Simulation	114
4.2.4	Rx Oscillator Momentum Co-Simulation	119
4.2.5	Tx Oscillator Calculation	123
4.2.6	Tx Oscillator Lump Component Model Simulation	124
4.2.7	Tx Oscillator RF Component Model Simulation	128
4.2.8	Tx Oscillator Momentum Co-Simulation	133

4.3	VCO Buffer and Pad Attenuator Design	137
4.3.1	Rx VCO Buffer with Pad Attenuator Lump Component Model Simulation	137
4.3.2	Rx VCO Buffer with Pad Attenuator RF Component Model Simulation	140
4.3.3	Rx VCO Buffer with Pad Attenuator Momentum Co- Simulation	143
4.3.4	Tx VCO Buffer with Pad Attenuator Lump Component Model Simulation	146
4.3.5	Tx VCO Buffer with Pad Attenuator RF Component Model Simulation	149
4.3.6	Tx VCO Buffer with Pad Attenuator Momentum Co- Simulation	152
4.4	Pre-Mixer Filter Design	155
4.4.1	Pre-Mixer Filter Calculation	155
4.4.2	Pre-Mixer Filter Lump Component Model Simulation	156
4.4.3	Pre-Mixer Filter RF Component Model Simulation	157
4.4.4	Pre-Mixer Filter Momentum Co-Simulation	158
4.5	VCO Design	159
4.5.1	Rx VCO RF Component Model Simulation	160
4.5.2	Rx VCO Momentum Co-Simulation	164
4.5.3	Tx VCO RF Component Model Simulation	168
4.5.4	Tx VCO Momentum Co-Simulation	172
4.6	Phase Noise Discussion	176
4.7	Summary	178

CHAPTER 5	RESULTS AND DISCUSSIONS	179
5.1	Introduction	179
5.2	Measurement Results and Discussion	180
5.2.1	Rx VCO Buffer with Pad Attenuator Measurement Results and Analysis	180
5.2.2	Pre-Mixer Filter Measurement Result and Analysis	183
5.2.3	Rx VCO Measurement Results and Analysis	184
5.2.4	Tx VCO Buffer with Pad Attenuator Measurement Results and Analysis	188
5.2.5	Tx VCO Measurement Results and Analysis	191
5.3	Competitive Analysis with Previous Works	195
5.4	Summary	195
CHAPTER 6	CONCLUSIONS AND FUTURE WORKS	197
6.1	Conclusions	197
6.2	Future Works	198
	LIST OF PUBLICATIONS	200
	REFERENCES	201
APPENDIX A:	ADS SIMULATOR	
APPENDIX B:	TOSHIBA HN1V02H VARACTOR DIODE DATASHEET	
APPENDIX C:	TOSHIBA HN1V02H VARACTOR DIODE SPICE DATA	
APPENDIX D:	ON SEMI MMBFU310LT1 JFET TRANSISTOR DATASHEET	
APPENDIX E:	PAD ATTENUATOR SIMULATION	

APPENDIX F: VHF LOW BAND VCO MEASURED PERFORMANCE AT
EXTREME TEMPERATURE

LIST OF TABLES

		PAGE
Table 1.1	Phase noise specifications of VCO	7
Table 1.2	ACR, ACP, Hum & Noise specifications (TIA, 2002)	8
Table 1.3	Design specifications of Rx VCO	9
Table 1.4	Design specifications of Tx VCO	9
Table 2.1	Previous works comparison for VCO operating in VHF range	55
Table 3.1	Electrical characteristics for HN1V02H	83
Table 3.2	Simulated varactor capacitance for the desired resonance frequency	84
Table 3.3	On characteristics of MMBFU310LT1	91
Table 3.4	Summarized comparison of simulated capacitance for varactor network with RFC, to linearizing inductor of 820 nH (a) and linearizing inductor of 1.2 μ H (b)	96
Table 4.1	Net capacitance of varactor diodes (a), inductor selection (b), and capacitors selection (c), for Rx oscillator design	107
Table 4.2	Calculated Rx oscillation frequency from the selected components value	108
Table 4.3	Rx oscillator performance simulated using lump component model	113
Table 4.4	Rx oscillator performance simulated using RF component model	118
Table 4.5	Rx oscillator performance simulated using Momentum	122

	co-simulation model	
Table 4.6	Net capacitance of varactor diodes (a), inductor selection (b), and capacitors selection (c), for Tx oscillator design	123
Table 4.7	Calculated Tx oscillation frequency from the selected component values	123
Table 4.8	Tx oscillator performance simulated using lump component model	128
Table 4.9	Tx oscillator performance simulated using RF component model	132
Table 4.10	Tx oscillator performance simulated using Momentum co-simulation model	136
Table 4.11	Parts reference for Rx VCO	161
Table 4.12	Rx VCO performance simulated using RF component model	163
Table 4.13	Rx VCO performance simulated using Momentum co-simulation model	167
Table 4.14	Parts reference for Tx VCO	169
Table 4.15	Tx VCO performance simulated using RF component model	171
Table 4.16	Tx VCO performance simulated using Momentum co-simulation model	175
Table 4.17	Rx oscillator phase noise comparison between low phase noise design and conventional design	177
Table 4.18	Tx oscillator phase noise comparison between low phase noise design and conventional design	177

Table 5.1	Rx VCO measured performance	184
Table 5.2	Tx VCO measured performance	191
Table 5.3	Phase noise comparison with other publications	195

LIST OF FIGURES

		PAGE
Figure 1.1	VCO used as LO in Rx and RF source in Tx (Zhu, 2005)	1
Figure 1.2	Block diagram of PLL (Zhu, 2005)	2
Figure 2.1	Spectral density of flicker noise versus (vs.) frequency	17
Figure 2.2	General RTN characteristic	17
Figure 2.3	An ideal oscillating signal in time domain and frequency domain	18
Figure 2.4	A practical oscillating signal in time domain and frequency domain	18
Figure 2.5	Phase noise referenced to the carrier frequency power in 1 Hz bandwidth	19
Figure 2.6	Effect of phase noise onto the wanted signal	20
Figure 2.7	SSB oscillator phase noise output spectrum	22
Figure 2.8	One-port negative resistance oscillator with noise current in the tank	23
Figure 2.9	Noise shaping in oscillators	25
Figure 2.10	Tank circuit includes the series parasitic resistance, R_l and R_c , as well as the parallel parasitic resistance, R_p	25
Figure 2.11	Impulse effects on a sinusoidal signal (Hajimiri and Lee, 1998)	28
Figure 2.12	ISF of an LC oscillator (Hajimiri and Lee, 1998)	29
Figure 2.13	Input voltage (top), output current (middle), and transconductance (bottom) of a bipolar differential pair	35

	biased by 1 mA tail current	
Figure 2.14	Dependence of AM and PM transconductance of a BJT (left) and MOS (right) pairs as a function of the amplitude of the input signal	38
Figure 2.15	Oscillator trajectories	42
Figure 2.16	Base and collector uncoupling with capacitor (Samori and Laicaita, 1998)	47
Figure 2.17	Capacitive filtering at the tail current source (Muer <i>et al.</i> , 2000)	49
Figure 2.18	Tail-biased oscillator with noise filter	50
Figure 2.19	Switched capacitor array design VCO	52
Figure 2.20	Set K_v curves by selecting MIM capacitors and tuning varactors	52
Figure 2.21	The differential steering voltage control design	53
Figure 2.22	The complementary capacitance to steering voltage characteristic	54
Figure 3.1	Design flow of low phase noise VCO for VHF low band	59
Figure 3.2	Tx and Rx VCO block design	61
Figure 3.3	Common-gate FET Colpitts oscillator topology	62
Figure 3.4	Common-gate FET Colpitts oscillator topologies in terms of impedance block (a) and small signal block model (b)	63
Figure 3.5	Close loop block model of the VCO	69
Figure 3.6	Open loop block model of the VCO	69
Figure 3.7	Summary of full-wave analysis (a) and quasi-static analysis (b)	72

Figure 3.8	Layout layer structure and thickness	75
Figure 3.9	Setting up the Hitachi halogen-free FR-4 substrate	75
Figure 3.10	Setting up the copper layer of the PCB	76
Figure 3.11	Via sheet in between the top conductor layer and the inner ground plane	77
Figure 3.12	Tx oscillator layout on the top layer (a) while the Rx oscillator layout on the bottom layer (b)	78
Figure 3.13	Rx buffer and pad attenuator layout on the top layer (a) while Tx buffer and pad attenuator layout are on the bottom layer (b)	78
Figure 3.14	Top (a) and bottom (b) layout of the Rx pre-mixer filter	78
Figure 3.15	Setup control for mesh computation	80
Figure 3.16	EM model of the oscillator layout (a), the buffer and pad attenuator layout (b), as well as the pre-mixer filter layout (c)	80
Figure 3.17	Component model of the oscillator layout (a), the buffer and pad attenuator layout (b), as well as the pre-mixer filter layout (c)	81
Figure 3.18	Simulation circuit for the HN1V02H capacitance, where the varactor is modeled base on the spice data from Toshiba	84
Figure 3.19	Varactor capacitance across the steering voltage, at 30 MHz to 57 MHz	84
Figure 3.20	Back-to-back varactor configuration	85
Figure 3.21	Forward biased and reverse biased regions of the varactor	85

Figure 3.22	S_{21} simulation setup for C1608X7R1H103K component model (a) as well as S_{21} simulation result	87
Figure 3.23	Z_{11} simulation setup for 1812CS-333XJLC component model (a) and 1812CS-273XJLC component model (b) as well as Z_{11} simulation result (c)	88
Figure 3.24	Z_{11} simulation setup for the FBMH4525-HM162NT component model (a) as well as Z_{11} simulation result (b)	89
Figure 3.25	MMBFU310LT1 forward transconductance vs. gate-source voltage plot	91
Figure 3.26	MMBFU310LT1 junction capacitance vs. gate-source voltage plot	91
Figure 3.27	MMBFU310LT1 common-gate S-parameter vs. frequency plot	92
Figure 3.28	Low noise biasing circuit design	92
Figure 3.29	Linearizing inductor connected to the back-to-back varactors	93
Figure 3.30	Simulation setup for the Rx VCO varactor network connected to RFC (a) and 820 nH linearizing inductor (c); Simulation setup for the Tx VCO varactor network connected to RFC (b) and 1.2 uH linearizing inductor (d)	95
Figure 3.31	Comparison of the back-to-back varactor capacitance connected with RFC, to that with linearizing inductor of 820 nH (a) and 1.2 μ H (b)	96
Figure 3.32	ON Semi MMBD353LT1 Schottky diodes act as AGC to the oscillator	97

Figure 3.33	S-parameter measurement setup	98
Figure 3.34	VCO parametric test setup	99
Figure 3.35	VCO frequency and sensitivity test setup	100
Figure 3.36	VCO output power and feedback power test setup	101
Figure 3.37	VCO hum & noise test setup	102
Figure 4.1	Oscillator design	105
Figure 4.2	Calculated Rx oscillator frequency response	108
Figure 4.3	Rx oscillator schematic designed using lump component model	109
Figure 4.4	S-parameter simulator setup for Rx oscillator lump component model	110
Figure 4.5	Rx oscillator open loop gain and phase shift plot for low (a) and high (b) end of the band, simulated using lump component model	111
Figure 4.6	HB simulator setup for Rx oscillator lump component model	111
Figure 4.7	Rx oscillator frequency response simulated using lump component model	112
Figure 4.8	Rx oscillator phase noise response simulated using lump component model	112
Figure 4.9	Rx oscillator output power and second harmonics simulated using lump component model	113
Figure 4.10	Rx oscillator schematic designed using RF component model	115
Figure 4.11	S-parameter simulator setup for Rx oscillator RF	116

	component model	
Figure 4.12	Rx oscillator open loop gain and phase shift plot for low (a) and high (b) end of the band, simulated using RF component model	116
Figure 4.13	HB simulator setup for Rx oscillator RF component model	117
Figure 4.14	Rx oscillator frequency response simulated using RF component model	117
Figure 4.15	Rx oscillator phase noise response simulated using RF component model	117
Figure 4.16	Rx oscillator output power and second harmonics simulated using RF component model	118
Figure 4.17	Rx oscillator schematic designed using Momentum co-simulation model	119
Figure 4.18	Rx oscillator open loop gain and phase shift plot for low (a) and high (b) end of the band, simulated using Momentum co-simulation model	120
Figure 4.19	Rx oscillator frequency response simulated using Momentum co-simulation model	121
Figure 4.20	Rx oscillator phase noise response simulated using Momentum co-simulation model	121
Figure 4.21	Rx oscillator output power and second harmonics simulated using Momentum co-simulation model	122
Figure 4.22	Calculated Tx oscillator frequency response	124
Figure 4.23	Tx oscillator schematic designed using lump component model	125

Figure 4.24	Tx oscillator open loop gain and phase shift plot for low (a) and high (b) end of the band, simulated using lump component model	126
Figure 4.25	Tx oscillator frequency response simulated using lump component model	126
Figure 4.26	Tx oscillator phase noise response simulated using lump component model	126
Figure 4.27	Tx oscillator output power and second harmonics simulated using lump component model	128
Figure 4.28	Tx oscillator schematic designed using RF component model	129
Figure 4.29	Tx oscillator open loop gain and phase shift plot for low (a) and high (b) end of the band, simulated using RF component model	130
Figure 4.30	Tx oscillator frequency response simulated using RF component model	131
Figure 4.31	Tx oscillator phase noise response simulated using RF component model	131
Figure 4.32	Tx oscillator output power and second harmonics simulated using RF component model	132
Figure 4.33	Tx oscillator schematic designed using Momentum co-simulation model	133
Figure 4.34	Tx oscillator open loop gain and phase shift plot for low (a) and high (b) end of the band, simulated using Momentum co-simulation model	134

Figure 4.35	Tx oscillator frequency response simulated using Momentum co-simulation model	135
Figure 4.36	Tx oscillator phase noise response simulated using Momentum co-simulation model	135
Figure 4.37	Tx oscillator output power and second harmonics simulated using RF component models	136
Figure 4.38	Schematic of Rx VCO buffer with pad attenuator designed using lump component model	138
Figure 4.39	LSSP simulator setup for Rx VCO buffer with pad attenuator using lump component model	138
Figure 4.40	Gain of Rx VCO buffer with pad attenuator simulated using lump component model	139
Figure 4.41	Isolation of Rx VCO buffer with pad attenuator simulated using lump component model	139
Figure 4.42	Stability plot of Rx VCO buffer with pad attenuator Simulated using lump component model	140
Figure 4.43	Output return loss of Rx VCO buffer with pad attenuator and buffer alone, simulated using lump component model	140
Figure 4.44	Schematic of Rx VCO buffer with pad attenuator designed using RF component model	141
Figure 4.45	LSSP simulator setup for Rx VCO buffer with pad attenuator using RF component model	141
Figure 4.46	Gain of Rx VCO buffer with pad attenuator simulated using RF component model	142
Figure 4.47	Stability plot of Rx VCO buffer with pad attenuator	142

	simulated using RF component model	
Figure 4.48	Isolation of Rx VCO buffer with pad attenuator simulated using RF component model	143
Figure 4.49	Output return loss of Rx VCO buffer with pad attenuator and buffer alone, simulated using RF component model	143
Figure 4.50	Schematic of Rx VCO buffer with pad attenuator designed using Momentum co-simulation model	144
Figure 4.51	Gain of Rx VCO buffer with pad attenuator simulated using Momentum co-simulation model	145
Figure 4.52	Stability plot of Rx VCO buffer with pad attenuator simulated using Momentum co-simulation model	145
Figure 4.53	Isolation of Rx VCO buffer with pad attenuator simulated using Momentum co-simulation model	146
Figure 4.54	Output return loss of Rx VCO buffer with pad attenuator and buffer alone, simulated using Momentum co-simulation model	146
Figure 4.55	Schematic of Tx VCO buffer with pad attenuator designed using lump component model	147
Figure 4.56	Insertion loss of Tx VCO buffer with pad attenuator simulated using lump component model	148
Figure 4.57	Isolation of Tx VCO buffer with pad attenuator simulated using lump component model	148
Figure 4.58	Stability plot of Tx VCO buffer with pad attenuator simulated using lump component model	148
Figure 4.59	Output return loss of Tx VCO buffer with pad attenuator	149

	and buffer alone, simulated using lump component model	
Figure 4.60	Schematic of Tx VCO buffer with pad attenuator designed using RF component model	149
Figure 4.61	Insertion loss of Tx VCO buffer with pad attenuator simulated using RF component model	150
Figure 4.62	Stability plot of Tx VCO buffer with pad attenuator simulated using RF component model	151
Figure 4.63	Isolation of Tx VCO buffer with pad attenuator simulated using RF component model	151
Figure 4.64	Output return loss of Tx VCO buffer with pad attenuator and buffer alone, simulated using RF component model	151
Figure 4.65	Schematic of Tx VCO buffer with pad attenuator designed using Momentum co-simulation model	152
Figure 4.66	Insertion loss of Tx VCO buffer with pad attenuator simulated using Momentum co-simulation model	153
Figure 4.67	Stability plot of Tx VCO buffer with pad attenuator simulated using Momentum co-simulation model	154
Figure 4.68	Isolation of Tx VCO buffer with pad attenuator simulated using Momentum co-simulation model	154
Figure 4.69	Output return loss of Tx VCO buffer with pad attenuator and buffer alone, simulated using Momentum co-simulation model	154
Figure 4.70	Calculated pre-mixer filter response	156
Figure 4.71	Pre-mixer filter schematic designed using lump component Model	157

Figure 4.72	LSSP simulator setup for pre-mixer filter using lump component model	157
Figure 4.73	Pre-mixer filter response simulated using lump component model	157
Figure 4.74	Pre-mixer filter schematic designed using RF component model	158
Figure 4.75	Pre-mixer filter response simulated using RF component model	158
Figure 4.76	Pre-mixer filter schematic designed using Momentum co-simulation model	158
Figure 4.77	Pre-mixer filter response simulated using Momentum co-simulation model	159
Figure 4.78	Rx VCO schematic designed using RF component model	161
Figure 4.79	Rx VCO frequency response simulated using RF component model	162
Figure 4.80	Rx VCO phase noise response simulated using RF component model	162
Figure 4.81	Rx VCO sensitivity simulated using RF component model	162
Figure 4.82	Rx VCO output power, feedback power, second harmonics simulated using RF component model	163
Figure 4.83	Rx VCO schematic designed using Momentum co-simulation model	165
Figure 4.84	Rx VCO frequency response simulated using Momentum co-simulation model	166
Figure 4.85	Rx VCO phase noise response simulated using Momentum	166

	co-simulation model	
Figure 4.86	Rx VCO sensitivity simulated using Momentum co-simulation model	166
Figure 4.87	Rx VCO output power, feedback power, second harmonics simulated using Momentum co-simulation model	167
Figure 4.88	Tx VCO schematic designed using RF component model	169
Figure 4.89	Tx VCO frequency response simulated using RF component model	170
Figure 4.90	Tx VCO phase noise response simulated using RF component model	170
Figure 4.91	Tx VCO sensitivity simulated using RF component model	170
Figure 4.92	Tx VCO output power, feedback power, second harmonics simulated using RF component model	171
Figure 4.93	Tx VCO schematic designed using Momentum co-simulation model	173
Figure 4.94	Tx VCO frequency response simulated using Momentum co-simulation model	174
Figure 4.95	Tx VCO phase noise response simulated using Momentum co-simulation model	174
Figure 4.96	Tx VCO sensitivity simulated using Momentum co-simulation model	174
Figure 4.97	Tx VCO output power, feedback power, second harmonics simulated using Momentum co-simulation model	175
Figure 4.98	Typical oscillator topology without RFC, RF bypass capacitor, and low noise biasing design	176

Figure 5.1	Mentor Graphics layout of Rx VCO (a) and Tx VCO (b)	179
Figure 5.2	Prototyped Rx VCO (a) and Tx VCO (b)	179
Figure 5.3	Comparison of measured and simulated output return loss for Rx VCO buffer with pad attenuator	181
Figure 5.4	Comparison of measured and simulated isolation for Rx VCO buffer with pad attenuator	181
Figure 5.5	Comparison of measured and simulated gain for Rx VCO buffer with pad attenuator	182
Figure 5.6	Comparison of measured and simulated stability factor K for Rx VCO buffer with pad attenuator	182
Figure 5.7	Comparison of measured and simulated pre-mixer filter response	183
Figure 5.8	Comparison of measured and simulated Rx VCO frequency response	185
Figure 5.9	Comparison of measured and simulated Rx VCO sensitivity	186
Figure 5.10	Comparison of measured and simulated Rx VCO phase noise at low end (a), middle (b), and high end (c) of the band	187
Figure 5.11	Comparison of measured and simulated output return loss for Tx VCO buffer with pad attenuator	189
Figure 5.12	Comparison of measured and simulated isolation for Tx VCO buffer with pad attenuator	189
Figure 5.13	Comparison of measured and simulated insertion loss for Tx VCO buffer with pad attenuator	190

Figure 5.14	Comparison of measured and simulated stability factor K for Tx VCO buffer with pad attenuator	190
Figure 5.15	Comparison of measured and simulated Tx VCO frequency response	192
Figure 5.16	Comparison of measured and simulated Tx VCO sensitivity	193
Figure 5.17	Comparison of measured and simulated Tx VCO phase noise at low end (a), middle (b), and high end (c) of the band	194

LIST OF ABBREVIATIONS

2 nd	Second
ACP	Adjacent Channel Power
ACR	Adjacent Channel Rejection
ADS	Advanced Design System
AGC	Automatic Gain Control
AM	Amplitude Modulation
BER	Bit Error Rate
BJT	Bipolar Junction Transistor
BOM	Bill of Material
C	Capacitor
CRT	Cathode Ray Tube
DC	Direct Current
Deg	Degree
DegC	Degree Celcius
DTV	Digital Television
EDA	Electronic Design Automation
EIA	Electronic Industries Aliance
EM	Electromagnetic
ESR	Effective Series Resistance
Etc.	Etcetera
FCC	Federal Communications Commission
FET	Field Effect Transistor
Fig.	Figure

FM	Frequency Modulation
Freq	Frequency
FR-4	Flame Retardant – Type 4
GDSII	Graphic Design System II
HB	Harmonic Balance
HP	Hewlett Packett
IC	Integrated Circuit
ISF	Impulse Sensitivity Function
JFET	Junction Field Effect Transistor
KCL	Kirchoff's Current Law
K _v	VCO sensitivity
KVL	Kirchoff's Voltage Law
L	Inductor
LC	Inductor-Capacitor
LNA	Low Noise Amplifier
LO	Local Oscillator
LSSP	Large Signal Scattering Parameter
LTI	Linear Time Invariant
LTV	Linear Time Variant
Max	Maximum
MIM	Metal-Insulator-Metal
Min	Minimum
MoM	Method of Moments
MOS	Metal Oxide Semiconductor
MOSFET	Metal Oxide Semiconductor Field Effect Transistor

No.	Number
NTI	Nonlinear Time-Invariant
PA	Power Amplifier
PCB	Printed Circuit Board
PLL	Phase-Locked Loop
PM	Phase Modulation
PN	Positive Negative
Q	Quality
RC	Resistor-Capacitor
Ref.	Reference
RF	Radio Frequency
RFC	Radio Frequency Choke
RHP	Right-half-plane
rms	root mean square
RTN	Random Telegraph Noise
Rx	Receiver
SCV	Sub-clutter Visibility
SM	Surface Mount
SMA	Sub-Miniature version A
S/N	Signal-to-Noise
SOLT	Short, Open, Load, Thru
S-parameter	Scattering Parameter
SRF	Self Resonance Frequency
SSB	Single Sideband
Temp	Temperature

TIA	Telecommunications Industry Association
Tx	Transmitter
US	United States
VCO	Voltage Controlled Oscillator
VHF	Very High Frequency
vs.	versus

**REKABENTUK OSILATOR KAWALAN VOLTAN (VCO) FREKUENSI
SANGAT TINGGI (VHF) ALUR RENDAH YANG BERFASA HINGAR
RENDAH UNTUK APLIKASI ALAT HUBUNG**

ABSTRAK

Penyelidikan teknologi alat hubung bagi Frekuensi Sangat Tinggi (VHF) alur rendah kini adalah kurang kerana sistem komunikasi hari ini banyak menggunakan alur frekuensi yang lebih tinggi. Sesungguhnya, alur rendah masih diperlukan dalam bidang tertentu, seperti keselamatan awam disebabkan lingkungannya yang luas dan tepat. Tesis ini menyelidiki peningkatan fasa hingar bagi Osilator Kawalan Voltan (VCO) alur rendah. Varaktor saling balik, induktor linearasi, dan jaringan bias hingar rendah telah dikemukakan. Penempatan tepat bagi kapasitor bypass, chok, dan manik ferit, juga pemilihan betul bagi bahagian lain dalam rekabentuk ini telah dipelajari dan dimasukkan. Rekabentuk penghantar VCO termasuk sebuah osilator diikuti dengan sebuah penyangga dan sebuah bantalan penurun. Rekabentuk penerima VCO adalah serupa tetapi ditambahkan dengan sebuah penapis pada pengeluarannya demi merendahkan harmonik sebelum dituju ke pencampur. Ko-simulasi Momentum telah diperkenalkan dan didapati lebih tepat dibandingkan dengan kaedah simulasi biasa. Fasa hingar penerima VCO yang dinilai adalah lebih kurang -126 dBc/Hz pada jarak 12.5 kHz dan lebih kurang -136 dBc/Hz pada jarak 25 kHz. Fasa hingar penghantar VCO yang dinilai adalah lebih kurang -134 dBc/Hz pada jarak 12.5 kHz dan lebih kurang -141 dBc/Hz pada jarak 25 kHz. Kedua-dua VCO telah menepati perincian, iaitu kurang daripada -118 dBc/Hz pada jarak 12.5 kHz dan kurang daripada -133 dBc/Hz pada jarak 25 kHz. VCO ini bersesuaian dalam aplikasi rumahtangga dan keselamatan awam.

**DESIGN OF LOW PHASE NOISE VERY HIGH FREQUENCY (VHF) LOW
BAND VOLTAGE CONTROLLED OSCILLATOR (VCO) FOR
TRANSCIVER APPLICATION**

ABSTRACT

There is little research in transceiver technology for Very High Frequency (VHF) low band nowadays because many communication systems today use higher frequency bands. However, low band is still required in specific fields, such as public safety due to its extensive and precise coverage. This thesis researches improvement in the phase noise of the low band Voltage Controlled Oscillator (VCO). As such, the back-to-back varactor, the linearizing inductor, and the low noise biasing network are introduced. Sensible placement of the bypass capacitor, choke, and ferrite bead as well as proper selection of parts have been studied and implemented. The transmitter VCO design comprises of an oscillator cascaded with a buffer and a pad attenuator to improve the output matching. The receiver VCO has a similar design but added with a filter at the output to suppress its harmonics before injected into the mixer. Momentum co-simulation is introduced and proven as a closer correlated simulation method compared to conventional simulations. The receiver VCO measured phase noise is around -126 dBc/Hz at 12.5 kHz offset and around -136 dBc/Hz at 25 kHz offset. The transmitter VCO measured phase noise is around -134 dBc/Hz at 12.5 kHz offset and around -141 dBc/Hz at 25 kHz offset. Both VCOs phase noise comply with the specifications of < -118 dBc/Hz at 12.5 kHz offset and < -133 dBc/Hz at 25 kHz offset. Such VCO is suitable in both domestic and public safety applications.

CHAPTER 1

INTRODUCTION

1.1 Background

The Voltage Controlled Oscillator (VCO) is often referred as the center operating engine of all transceiver systems as it is shared by both the receiver (Rx), as Local Oscillator (LO), and by the transmitter (Tx), as Radio Frequency (RF) source, as shown in Fig. 1.1. Therefore, very stringent requirements are placed on the spectral purity of VCOs, making its design a critical sub-circuit to the overall transceiver system performance. Being the block model within the Phase Locked Loop (PLL) which generates oscillation frequency, as depicted in Fig. 1.2, the design of VCO is a major challenge and has thus extensively been researched over the past decades, as evidenced by the large number of publications (Craninckx and Steyaert, 1995a; Craninckx and Steyaert, 1995b; Craninckx and Steyaert, 1997; Samori *et al.*, 1998a; Samori and Laicaita, 1998b; Zannoth *et al.*, 1998; Margarit *et al.*, 1999; Hegazi, Sjoland and Abidi, 2001; Zanchi *et al.*, 2001; Tiebout, 2001; Fong *et al.*, 2003; Perticaroli, Palma and Carbone, 2011).

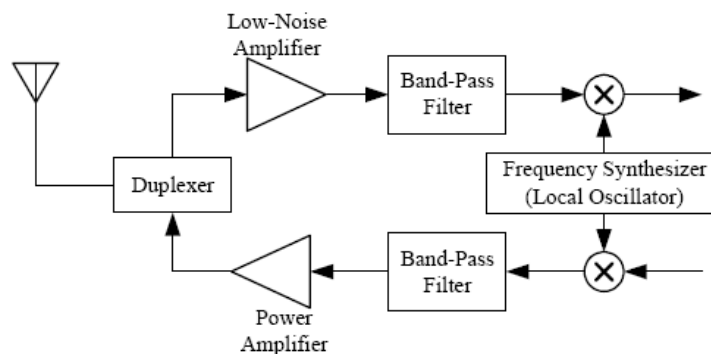


Figure 1.1: VCO used as LO in Rx and RF source in Tx (Zhu, 2005)

The electromagnetic (EM) spectrum is the total range of frequencies of EM radiation. It extends from the audio waves (15 Hz) to the light waves (900000 GHz). The range of spectrum frequencies used for broadcast communications is called the “broadcast frequency spectrum”. This spectrum is split into bands, in which the Very High Frequency (VHF) low band, or also known as ‘low band’, ranges from 25 MHz to 50 MHz.

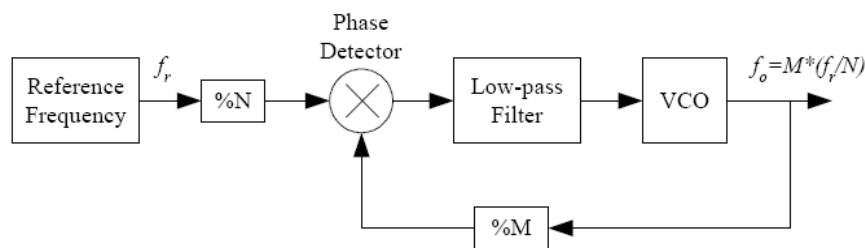


Figure 1.2: Block diagram of PLL (Zhu, 2005)

1.2 Applications of VHF Low Band

In the United States (US), the Federal Communications Commission (FCC) controls RF assignments for non-governmental use. The FCC has divided up the available frequencies into different groups and assigned each group to a specific use. The VHF low band is among the 5 primary bands which the FCC has reserved for exclusive use by the public safety agencies. For instance, many fire agencies in New York, New Hampshire, Pennsylvania, and Maine rely on low band operations due to the excellent coverage and range achievable in this band (Low Band, 2005).

Under the FCC rules, any organization and individual that provides some type of public safety mission can be assigned frequencies from this Public Safety Radio Pool. Such qualifying organization and individual include: police, fire, emergency medical services, veterinarians, animal hospitals, disaster relief

organizations, blood banks, heart and lung centers, school bus services, botanical gardens, departments of agricultures and environmental resources, beach patrols, retirement facilities and home for the aged, mental health institutions, rehabilitation centers, electric power cooperatives, state reservations and tribal councils, Universities, water control boards, as well as emergency repair services for public communications facilities (Veeneman, 2002).

1.3 Advantages of VHF Low Band

While today's communication trend seems to be migrating towards the higher spectrum from 800/900 MHz to a few GHz, it remains a fact that the VHF low band is still popularly used in the community, even still, the popularity continues to grow rapidly. Such popularity in usage relies much on the many advantages available in low band, which is yet irreplaceable by any of the higher band (Low Band, 2005).

1.3.1 Precise Transmission

The atmosphere that surrounds the earth acts to attenuate and refract radio signals. The magnitude of attenuation and refraction depends on the frequency of the signal. The lower is the frequency, the less the attenuation, or loss of signal. VHF low band has such a precise area of broadcast because the ionosphere does not usually reflect the signal far beyond its immediate surroundings. Communication is thus optimal for reaching a target in close vicinity without interfering with broadcasts. Unlike the higher frequencies, low band signal is not obscured by buildings or tarnished by naturalistic sounds in the atmosphere, or by conflicting signals from nearby equipments (Mateo, 1999).

1.3.2 Extensive Coverage

One major advantage is the extensive effect it has on range. Each agency has a particular geographic area, in which they need solid radio coverage. VHF low band signals travel farther than higher frequencies because low band frequencies tend to follow the curvature of the earth. Rural businesses, farming operations, towing companies, and other uses that need service over a wide area will find that low band is an excellent choice for dependable radio communications. This is because rural areas usually have small buildings and a large geographic area to cover (Frequency and Spectrum, 2008).

1.3.3 Ample Spectrum Availability

Channel loading is a term used to describe the number of users assigned to the same frequency. Channel loading is so heavy in some areas that additional users are no longer allowed on particular channels. As many applications today have migrated to 800/900 MHz operations, there is ample spectrum available at VHF low band, greatly simplifying the frequency coordination effort and shortening the overall licensing procedure. Furthermore, the FCC declared that all television programming have to be switched to digital technology in 2009, this enables system operators to consolidate the information that was being broadcast for television and free up low band frequency (Frequency and Spectrum, 2008).

1.3.4 Exemption from Narrow Band Requirements

In an effort to improve spectral efficiency, the FCC has mandated that all new licenses granted after Jan 1, 2011 must be narrowband, for public safety agencies and business users. All of these systems must be converted or relicensed to narrowband

operation by Jan 1, 2013. However, this rule only applies for operation from 150 MHz to 512 MHz. VHF low band systems are exempted from such requirement, meaning that low band equipment put into service today will not become obsolete in 2013. So, low band makes sense for those agencies and businesses that need new systems or expansions of operations (Veeneman, 2002).

1.4 Problem Statement

As stated in Section 1.3, current communication is advancing towards the higher frequency bands, as a result, most research effort today is conducted on developing a low noise VCO in the GHz range (Lee *et al.*, 2011; Huang and Mao, 2011; Ham and Hajimiri, 2000; Yu, Meng and Lu, 2002; Li, 2003; Badillo and Kiaei, 2003; Eo, Kim and Oh, 2003; Hamano, Kawakam and Takagi, 2003). Research conducted on VHF low band remains little due to its limited application which is required only in specific field, such as public safety. Nonetheless, phase noise research in this band is critical because noise tends to occur in low frequencies. This is especially true for radiant energy, which can interfere with, and even blockade low band signals. According to the FCC, the most common sources of low band noise are industrial equipments, power lines, and home appliances, such as microwaves, vacuum cleaners, and dimmers (Frequency and Spectrum, 2008).

Phase noise is one of the major limiting factors affecting the VCO performance. Any system that requires a VCO for reference frequency generation can suffer from it. Phase noise directly affects short-term frequency stability, Bit-Error-Rate (BER), Signal to Noise and Distortion (SINAD), Adjacent Channel Rejection (ACR) for Rx, and Adjacent Channel Power (ACP) for Tx. Phase and fluctuation has therefore long been the subject of theoretical and experimental

investigation (Lee *et al.*, 2011; Huang and Mao, 2011; Baghdady, Lincoln and Nelin, 1965; Cutler and Searle, 1966; Leeson, 1966; Rutman, 1978; Abidi and Meyer, 1983; Weigandt, Kim and Gray, 1994; McNeil, 1994; Craninckx and Steyaert, 1995a; Craninckx and Steyaert, 1995b; Razavi, 1996). The ultimate goal of designing a perfect VCO is to produce a signal whose spectrum would consist of a single line of infinitesimal width. In reality, no perfect VCO has yet been discovered and virtually impossible so it seems, for all oscillators universally exhibit line width broadening of varying degree in their output power spectra. Such line width broadening produces phase noise, and is caused by noise inherent in the oscillator.

The accuracy in signal transmission is extremely crucial in ensuring instant and valid information is properly communicated. Improvement in phase noise results in substantial BER improvement of all communications. For all Doppler radar designs, improving the Sub-Clutter Visibility (SCV) is the bottom line, as this allows the radar to see small moving objects in the screen. Improving the phase noise increases the cancelled Signal-to-Noise (S/N) ratio, thereby improving the SCV. Low phase noise is also a key element in a missile illuminator as a signal injection with poor phase noise can result in the loss of the intended target in aim.

1.5 Research Objectives

The objectives of this research are:

- To design and propose a VCO design with low phase noise, so that when incorporated into a transceiver system, the ACR, ACP, and Hum & Noise of the system would comply with the Telecommunications Industry Association / Electronic Industries Alliance (TIA/EIA-603-B) standard (TIA, 2002).

- To study a better simulation technique using the Advanced Design System (ADS) Momentum co-simulation, that is more precise and co-related.
- To implement and characterize the proposed VCO design with main concentration on the evaluation of the phase noise parameter.

1.6 Requirements

The requirements for the researched VCO are

- To design a low phase noise VCO which is able to meet the specifications listed in Table 1.1.

Table 1.1: Phase noise specifications of VCO

Parameter	Freq Offset (kHz)	At Room Temperature
		25 deg C
Phase Noise (dBc/Hz)	12.5	< -118
	25	< -130

Phase noise proportionally affects the ACR, ACP, and Hum & Noise parameters of a transceiver system. FCC adopts the TIA/EIA-603-B standard, whereby Table 1.2 lists an excerpt of the TIA/EIA-603-B specifications for the affected parameters. ACR is defined as the ratio of the level of an unwanted input signal that causes the SINAD produced by a wanted signal 3 dB in excess of the reference sensitivity to be reduced to the standard SINAD, to reference sensitivity (TIA, 2002). The Rx VCO phase noise specification is approximated from the ACR specification, as

$$Phase_Noise = -ACR - SINAD - Attn_{IF_Filter}, \quad (1.1)$$

where $Phase_Noise$ is the phase noise specification, ACR is the ACR specification as listed in Table 1.2, $SINAD$ is 15 dB, which is the sum of the 12 dB reference with the 3 dB excess margins, and $Attn_{IF_Filter}$ is the attenuation of the Intermediate Frequency (IF) filter, which is about 54 dB for the 270 kHz bandwidth ceramic IF filter of a low band Rx system. Similarly, ACP is defined as the ratio of the total output power of a Tx system under defined conditions and modulation, to that part of the output power that falls within a specified pass band centered on the nominal frequency of either of the adjacent channel or channels further offset above or below the assigned carrier frequency. The Tx VCO phase noise specification is approximated from the ACP specification, as

$$Phase_Noise = ACP - Tx_Amp - 10 \log(f_{offset}), \quad (1.2)$$

where ACP specification as listed in Table 1.2, Tx_Amp is the gain in the low band Tx system, which is around 16 dB, and f_{offset} is the offset from the carrier frequency.

Table 1.2: ACR, ACP, Hum & Noise specifications (TIA, 2002)

Parameter	Offset (kHz)	Specifications (25 degC)
Rx Adjacent Channel Rejection (ACR)	12.5	> 50 dB
	25	> 60 dB
Tx Adjacent Channel Power (ACP)	12.5	< -60 dB
	25	< -70 dB
Hum & Noise	12.5	< -34 dB
	25	< -40 dB

- To design a Rx VCO that is able to meet the requirements in Table 1.3.

Table 1.3: Design specifications of Rx VCO.

	Specifications
LO Freq Range (MHz)	46.7 – 52.7
Lower End Guard Band (MHz)	> 3
Higher End Guard Band (MHz)	> 3
Oscillator Output Power (dBm)	> 14
Oscillator 2nd Harmonics Output Attenuation (dBc)	> 44
Feedback Output Power (dBm)	> 0
Phase Noise at 12.5kHz (dBc/Hz)	< -118
Phase Noise at 25kHz (dBc/Hz)	< -130
Hum & Noise at 12.5kHz (dB)	< -34
Hum & Noise at 25kHz (dB)	< -40

The requirements are developed from the Rx system of a public safety transceiver, such that the Rx VCO is able to integrate into the system as a LO that supports a high side injection for a bandwidth of 36 MHz to 42 MHz, and to produce a 10.7 MHz IF signal when down converted through a mixer.

- To design a Tx VCO that is able to meet the requirements in Table 1.4.

Table 1.4: Design specifications of the Tx VCO.

	Specifications
Freq Range (MHz)	36 – 42
Lower End Guard Band (MHz)	> 3
Higher End Guard Band (MHz)	> 3
Oscillator Output Power (dBm)	> 3
Oscillator 2nd Harmonics Output Attenuation (dBc)	> 15
Feedback Output Power (dBm)	> 0
Phase Noise at 12.5kHz (dBc/Hz)	< -118
Phase Noise at 25kHz (dBc/Hz)	< -130
Hum & Noise at 12.5kHz (dB)	< -34
Hum & Noise at 25kHz (dB)	< -40

The requirements are developed from the Tx system of a public safety transceiver, such that the Tx VCO is able to integrate into the system as a modulating source in which the signal is injected into the power amplifier (PA).

1.7 Research Scopes and Limitations

The research scopes and limitations are outlined as follows:

- To design the VCO oscillator, through theoretical calculation.
- To design the VCO oscillator, with ADS Scattering Parameter (S-parameter) and Harmonic Balance (HB) simulation, using different component models: lump component model, RF component model, and Momentum co-simulation model.
- To design the VCO buffer and pad attenuator, with ADS Large Signal S-parameter (LSSP) simulation, using different component models: RF component model and Momentum co-simulation model.
- To implement and evaluate the VCO buffer and pad attenuator. The co-relativity of the simulated results to the actual measured results is analyzed.
- To design the Rx pre-mixer low pass filter, through theoretical calculation.
- To design the Rx pre-mixer low pass filter, with ADS LSSP simulation, using different component models: lump component model, RF component model, and Momentum co-simulation model.
- To implement and evaluate Rx pre-mixer low pass filter. The co-relativity of the simulated results to the actual measured results is analyzed.

- To design and implement the Rx VCO. The co-relativity of the simulated results to the actual measured results is analyzed.
- To design and implement the Tx VCO. The co-relativity of the simulated results to the actual measured results is analyzed.
- The research only focuses on the phase noise improvement of the VCO.
- The bandwidth of the VCO is limited to 6 MHz according to the operating bandwidth in the low band range required for a public safety transceiver unit.
- Other limitations encountered in this research include the Printed Circuit Board (PCB) fabrication technology, the components placed, as well as the equipments applied for evaluation.

1.8 Research Contribution

Using the low-phase-noise design technique, which is detailed in Chapter 3, both the Rx and Tx VCOs designed in this research are able to generate RF signals of remarkably low phase noise level, in which, when incorporated into a transceiver system, would be able to comply with the FCC specifications. Thereby, the major contribution of this research is to support two-way communication systems and base stations, used in the public safety pool in the US, as well as other countries adopting such specifications. Despite this, other contributions of this research are as follows:

- By disabling the Tx VCO, the design could operate as a single Rx VCO, and vice versa. Single way communications applying only either VCO include broadcast systems, radar systems, missile illuminators etc.
- Unlike S-parameter simulation, co-relativity for HB simulation has long been an issue. Noises in VCO as well as parts parasitic are highly

unpredictable. This research provides an improved simulation method in predicting the performance of a VCO design. This, in turn, contributes to cycle time and cost reduction for the design.

- The VCO buffer and attenuator designs could be used as reference for oscillator as well as RF amplifier designs of other frequency bands.

1.9 Thesis Organization

This thesis is organized into six chapters to cover the entire research work and the theory related to the design. In chapter 2, literature review is detailed. This chapter documents the theory of noise in VCO, the development of various phase noise models, as well as methods in phase noise reduction.

Chapter 3 explains the methodology of the research. This includes the derivation of the mathematical model for the common gate Field Effect Transistor (FET) Colpitts oscillator, the overview of ADS simulation, and selection of components. The test methodology in evaluating the prototype is also detailed.

Chapter 4 describes the design and simulation of the VCO, which covers the oscillator circuitry, the buffer and pad attenuator circuitries, as well as the Rx pre-mixer low pass filter circuitry.

Chapter 5 reports the measured results of the hardware and further compares and discusses the data with the simulated results. The phase noise performance of the design is further analyzed and detailed in this chapter.

Finally, in chapter 6, the overall performance and findings of the research is concluded. Future work is recommended for further improvement of the design.

CHAPTER 2

LITERATURE SURVEY

2.0 Introduction

Resonance signal generated by oscillators suffer from fluctuations in both amplitude and phase. Such fluctuations are caused by internal noise generated by the components as well as external interference. Fluctuation in amplitude tends to be suppressed by the nonlinear characteristics of the oscillator; however, phase fluctuation is accumulated over a period of time. Phase fluctuation, also referred to as phase noise, has hence, been the key interest to researchers. Several models have been developed to formulate a more accurate phase noise performance and shall be detailed in this chapter. The characteristics of phase noise as well as other noises affecting the oscillator, with methods in noise reduction are also well elaborated.

2.1 Noise

The major source of noise in an oscillator is the active device, usually the transistor. The noise sources in any oscillator circuit ultimately combine to form amplitude modulation (AM) noise and phase modulation (PM) noise. The AM noise component is usually ignored because the gain limiting effects of the circuit control the output amplitude, allowing little variation due to noise. The PM noise is of great concern because its magnitude is typically greater than the AM noise contribution and directly affects the frequency stability of the oscillator (Siweris and Schiek, 1985) and related noise sidebands.

The designer has limited control over the noise sources in a transistor. For example, the bulk resistance of a transistor, upon which thermal noise depends on, is

an unchangeable, intrinsic property of the device. However, using knowledge on how noise affects oscillator waveforms, the designer is able to substantially improve phase-noise performance by the selection of bias point and signal level. The main mechanisms for noise in a semiconductor device include both thermal fluctuations in minority carrier flow as well as bulk and depletion area generation-combination events (Buckingham, 1983). The effects of these processes are categorized as thermal noise, shot noise, partition noise, burst noise, and flicker noise.

2.1.1 Thermal Noise

At any temperature above absolute zero, thermal agitation causes electrons in any conductor or semiconductor to be moving at random. At any one instant of time, the electrons may be concentrated in some areas more than others. These concentrations produce thermal noise. Thermal noise is generated by the random thermal motion of the electrons and is unaffected by Direct Current (DC), since typical electron drift velocities in a conductor are much less than thermal electron velocities. In a resistor R , thermal noise can be represented by a series voltage with the spectral density of

$$\frac{\overline{V^2}}{\Delta f} = 4kTR, \quad (2.1)$$

where k is the Boltzmann's constant, T is the absolute temperature in $^{\circ}\text{K}$, and Δf is the bandwidth (Manasse, Ekiss and Gray, 1967). Thermal noise is present in any linear passive device. In bipolar devices, the parasitic resistors can generate the thermal noise. For Metal Oxide Semiconductor Field Effect Transistors (MOSFETs),

the resistance of the channel also generates thermal noise with the spectral density given by

$$\frac{\overline{V^2}}{\Delta f} = \frac{2}{3} \cdot \frac{4kT}{g_m}, \quad (2.2)$$

where g_m is the conductance of the channel (Razavi, 2001).

2.1.2 Shot Noise

Shot noise is associated with a DC and is presented majorly in diodes and transistors. It is the fluctuation of the DC and is usually modeled as a noise current source with the spectral density of

$$\frac{\overline{I^2}}{\Delta f} = 2qI, \quad (2.3)$$

where q is the charge of an electron, I is the DC, and Δf is the bandwidth (Spangenburg, 1957).

In transistors, each current path will have its own associated shot noise. For example, a Bipolar Junction Transistor (BJT) has shot noise for each of the emitter, base, and collector currents (Thornton, 1966). An additional source of noise resulting from shot noise is called partition noise. Partition noise occurs at current junctions and is caused by each electron in making a decision to go one way or another. A statistical fluctuation in the collector and base currents equating to noise occurs (Krauss, Bostian and Raab, 1980). In a BJT, the majority of electrons flow from the emitter into the collector. A fraction of the emitter current must also flow to the base.

The splitting of the emitter current into the base and collector current components provides this basic partition noise contribution.

2.1.3 Flicker Noise

Flicker noise is found in all active devices as well as in some discrete passive elements. It is not a broadband phenomenon like thermal and shot noise; in fact, it is mainly caused by traps associated with contamination and crystal defects. The flicker noise is also called as $1/f$ noise because it displays a spectral density of the form

$$\frac{\overline{I^2}}{\Delta f} = K_1 \frac{I^a}{f^b}, \quad (2.4)$$

where I is the DC, K_1 , a , and b , are constants. The nonlinear performance of oscillators transforms this low frequency $1/f$ by up-conversions into the near-sidebands of the fundamental oscillation signal. The spectrum of $1/f$ noise varies inversely with frequency and thus is only noticeable at low frequencies and near sidebands. The low frequency performance is shown in Fig. 2.1. The upper frequency at which the $1/f$ noise sinks into the noise floor caused by thermal and shot noise is called $1/f$ corner frequency. This corner frequency is typically between 100 Hz to 1 MHz and the low frequency limit of $1/f$ noise has been followed to 10^{-7} Hz.

A contributor to $1/f$ in a device is called Random Telegraph Noise (RTN), also known as burst noise. RTN is the observed phenomenon whereby device current switches between several discrete values at random times. RTN is closely linked with $1/f$ noise in that it has spectral components which contribute to low frequency

noise (Kogan, 1966). A plot showing the RTN noise characteristics is shown in Fig. 2.2.

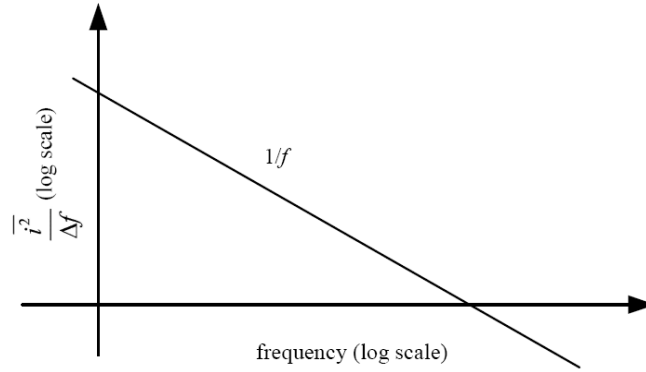


Figure 2.1: Spectral density of flicker noise versus (vs.) frequency

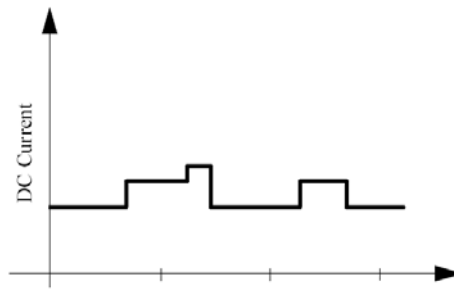


Figure 2.2: General RTN characteristic

2.2 Phase Noise

The signal shown in Fig. 2.3 is an ideal oscillating signal produced by an ideal oscillator, in which the signal as a function of time is

$$V_{out}(t) = V_o \cos[\omega_o t], \quad (2.5)$$

where V_o is the nominal amplitude and ω_o is the nominal frequency at time t . In frequency domain, this signal is presented by a single spectral line. However, in

practical oscillation system, the instantaneous frequency and magnitude of oscillation are not constant. These will fluctuate as a function of time as

$$V_{out}(t) = [V_o + E(t)]\cos[\omega_o t + \phi_o], \quad (2.6)$$

where $E(t)$ is the random amplitude fluctuations and ϕ_o is the random phase fluctuations. In frequency domain, the signal is no longer a discrete spectral line; rather, a spread of spectral lines both above and below the nominal signal frequency, as shown in Fig. 2.4, in the form of modulation sidebands due to the random fluctuations in phase and amplitude.

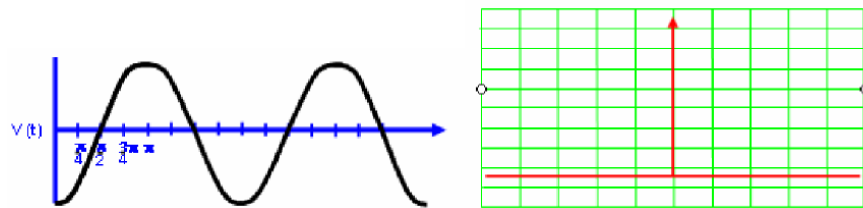


Figure 2.3: An ideal oscillating signal in time domain and frequency domain

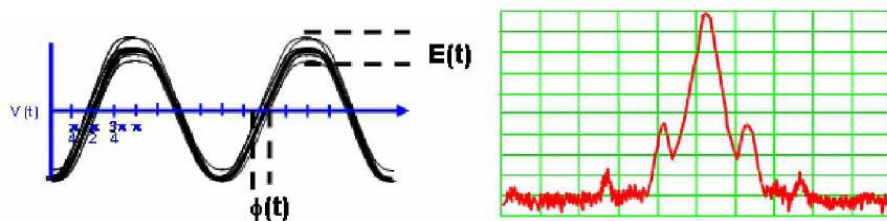


Figure 2.4: A practical oscillating signal in time domain and frequency domain

These modulation sidebands are generally referred to as phase noise sidebands (Xie *et al.*, 1998) and are usually characterized in terms of the single sideband (SSB) noise spectral density. It is defined as the SSB power due to phase fluctuations

referenced to the carrier frequency power in 1 Hz bandwidth at a specific offset frequency from the carrier divided by the signal's total power, with unit dBc/Hz:

$$L\{\Delta\omega\} = 10 \cdot \log \left[\frac{P_{sideband}(\omega_o + \Delta\omega, 1 \text{ Hz})}{P_{carrier}} \right], \quad (2.7)$$

where $P_{sideband}(\omega_o + \Delta\omega, 1 \text{ Hz})$ represents the SSB power at a frequency offset of $\Delta\omega$ from the carrier with a measurement bandwidth of 1 Hz as visualized in Fig. 2.5, and $P_{carrier}$ is the power of the carrier signal.

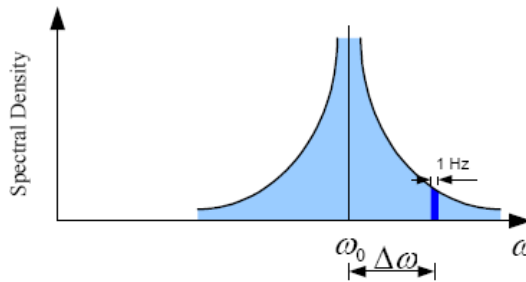


Figure 2.5: Phase noise referenced to the carrier frequency power in 1 Hz bandwidth

The advantage of this parameter is its ease of measurement. Its disadvantage is that it shows the sum of both amplitude and phase variations. However, it is important to understand the amplitude and phase noise separately because they behave differently in the circuitry. For instance, the effect of amplitude noise is reduced by the intrinsic amplitude limiting mechanism in oscillators and can be practically eliminated by the application of a limiter to the output signal, while the phase noise cannot be reduced in the same manner.

The destructive effect of phase noise can be significantly seen in the front-end of a super-heterodyne transceiver. Recapitulating the transceiver block diagram

in Fig. 1.1, the LO that provides the carrier signal for both mixers is embedded in a frequency synthesizer. If the LO is noisy, both the down-converted and up-converted signals are corrupted. As shown in Fig. 2.6, a large interferer in an adjacent channel may accompany the wanted signal. When two signals are mixed with the LO output exhibiting phase noise, the down-converted band consists of two overlapping spectra, with the wanted signal suffering from significant noise due to the tail of the interferer signal. This effect is referred to as “reciprocal mixing” (Krafcsik and Dawson, 1986). Therefore the output spectrum of a LO has to be extremely sharp. Such stringent requirements impose a great challenge in low-noise oscillator design.

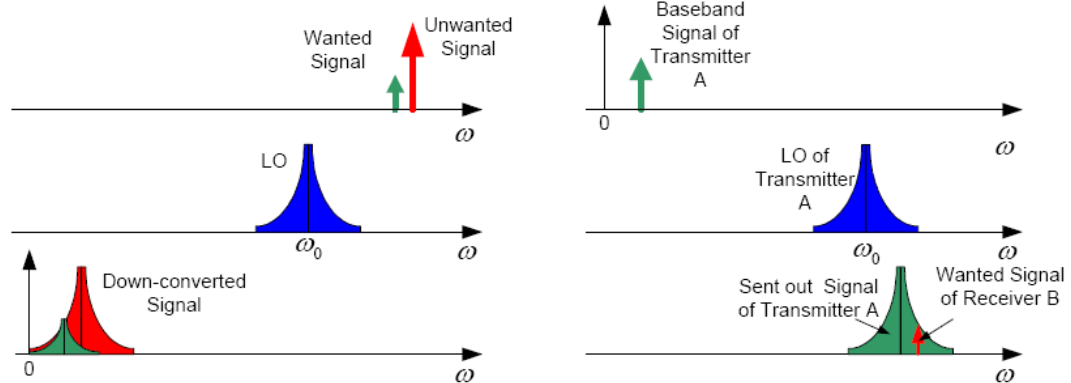


Figure 2.6: Effect of phase noise onto the wanted signal

Over the years, several phase noise models have been studied and developed to predict the phase noise performance of the oscillator and, thus, in pursuance of further improvement. Some of the commonly used models are detailed in the following sub-sections.

2.2.1 Leeson’s Model

D. B. Leeson proposed an empirical phase noise model to describe the phase noise depicted in Fig. 2.7. Noise prediction using Leeson’s model (1966) is based on

the time-invariant properties of the oscillator such as the resonator Quality (Q), feedback gain, output power, and noise figure. According to this model, the phase noise generated by an oscillator can be expressed as:

$$L\{\Delta\omega\} = 10 \cdot \log \left\{ \frac{2FkT}{P_s} \cdot \left[1 + \left(\frac{\omega_o}{2Q_L\Delta\omega} \right)^2 \right] \cdot \left[1 + \frac{\Delta\omega_{1/f^3}}{|\Delta\omega|} \right] \right\}, \quad (2.8)$$

where $L\{\Delta\omega\}$ is SSB noise spectra density in units of dBc/Hz. The symbol k is the Boltzmann's constant, T is the absolute temperature in ^0K , P_s is the carrier power, ω_o is the oscillation frequency, and $\Delta\omega$ is the offset frequency from ω_o . Q_L is the loaded Q of the oscillator resonator, F is the noise figure of the oscillator, and $\Delta\omega_{1/f^3}$ is the corner frequency between $1/f^2$ and $1/f^3$ region.

As shown in Fig. 2.7, the general phase noise output spectrum of an oscillator consists of 3 distinct sections allocated in the sideband. Immediately surrounding the carrier frequency there exists a region of noise which decay as $1/f^3$. At some frequency offset called the $1/f^3 - 1/f^2$ corner frequency, the noise spectrum changes to a $1/f^2$ dependence. The $1/f^2$ region continues on to the phase noise floor of the circuit. The noise floor of the circuit is a result of thermal and shot noise sources. The noise floor exists across all frequencies, even in the $1/f^2$ and $1/f^3$ region. The relative power associated with each section depends on each section's corner frequency and the noise floor level. The $1/f^2$ region is unavoidable as it is a result of the characteristics of the resonator. Any Inductor-Capacitor (LC) resonator will have a voltage dependence which varies as $1/f$ from the center frequency. Since power is proportional to voltage squared, the resulting power spectrum is

therefore $1/f^2$. The $1/f^3$ region comes from up-converted $1/f$ noise of the device. The $1/f^3$ dependency appears when $1/f$ is multiplied by the $1/f^2$ characteristic of the resonator.

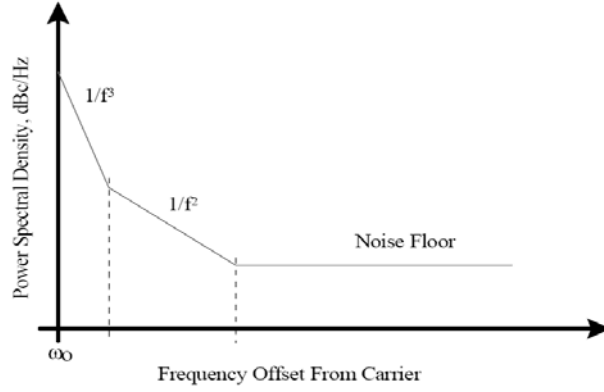


Figure 2.7: SSB oscillator phase noise output spectrum

In Leeson's model, $\Delta\omega_{1/f^3}$ is equal to the $1/f$ noise corner frequency of the device. In practice, however, $\Delta\omega_{1/f^3}$ is rarely equal to the $1/f$ noise corner frequency of the device. An existing problem is that the noise figure of an oscillator is extremely difficult to predict (Robins, 1982). The factor F remains a co-relation factor which can only be determined by measurement of the phase noise spectrum of the oscillator. Since F and $\Delta\omega_{1/f^3}$ must almost always be measured from the oscillator spectrum, the predictive power of Equation 2.8 is quite limited. From Equation 2.8, it can be seen that the corner frequency at which the $1/f^2$ sinks into the noise floor is exactly equal to the resonator half bandwidth, $\omega_o/2Q$. This also is not completely justifiable.

In short, according to Leeson's model, the only way to improve $L\{\Delta\omega\}$ is to increase the output power or increase the loaded Q of the resonator. The oscillator

must be designed in such a way that the transistor does not saturate. Saturation lowers the Q of the entire oscillator circuit, thus increasing phase noise and harmonics level (Rhea, 1990).

2.2.2 Linear Time Invariant (LTI) Model

It is convenient to model an LC cross-coupled oscillator as a one-port negative resistance model as shown in Fig. 2.8. In this model, the transconductance of the active circuit, G_m , must compensate for the loss caused by the parasitic resistance, R_p , in the tank, which is simply modeled as a parallel resistor.

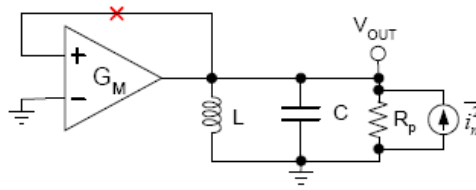


Figure 2.8: One-port negative resistance oscillator with noise current in the tank

The thermal noise it generates, is modeled as a noise current, $\overline{i_n^2}$, parallel with the tank. The thermal noise introduces the phase noise at the output of the oscillator. The transfer function from the noise current to the output voltage in closed-loop operations is derived as

$$T_{noise, R_p}^2(s) = \frac{\overline{V_n^2}}{\overline{i_n^2}} = \left[\frac{sL}{1 - sL(G_m - 1/R_p) + s^2LC} \right]^2, \quad (2.9)$$

where $T_{noise, R_p}^2(s)$ is the transfer function of the phase noise of the oscillator and $\overline{V_n^2}$ is the output voltage. With $G_m = I/R_p$, it can be shown that the transfer function at small offset frequency, $\Delta\omega$, is approximated as (Craninckx and Steyaert, 1995).

$$T_{noise, R_p}^2(\Delta\omega) = \left[\frac{I}{2j} \cdot \sqrt{\frac{L}{C}} \cdot \frac{\omega_o}{\Delta\omega} \right]^2, \quad (2.10)$$

where T_{noise, R_p}^2 is the equivalent impedance of the tank at the frequency $\omega_o \pm \Delta\omega$.

Accordingly, the one-side spectral density of the output noise voltage is

$$\overline{V_{on, g_p}^2}(\Delta\omega) = 4kTg_p \cdot \left(\frac{\omega_o}{2\Delta\omega} \right) \cdot (\omega_o^2 L^2), \quad (2.11)$$

where $\overline{V_{on, g_p}^2}(\Delta\omega)$ is the output noise voltage at offset frequency $\Delta\omega$ and g_p is the conductance, that is $g_p = I/R_p$. The noise voltage described here actually includes both the amplitude noise (AM noise) and the phase noise (PM noise). If the oscillator employs an Automatic Gain Control (AGC) circuit, the AM noise will be removed for frequency offset less than the AGC bandwidth. In addition, the nonlinearity of the oscillator determines oscillation amplitude and it can be viewed as an internal AGC mechanism in oscillators. Therefore, even when there is AM noise, it will decay away with time and thus has little effect on output phase noise. Neglecting the AM noise results in a 0.5 factor multiplied to Equation 2.11. So, the spectral density of the noise voltage is